Dalton Transactions

Accepted Manuscript

ROYAL SOCIETY OF CHEMISTRY

www.rsc.org/dalton

On the use of speciation techniques and ab initio modelling to understand tetravalent actinide behavior in biological medium: An^{IV}DTPA case

J. Aupiais *(1), L. Bonin (2), C. Den Auwer (3), P. Moisy (2), B. Siberchicot (1), S. Topin (1)

(1) CEA, DAM, DIF, F-91297 Arpajon cedex

(2) CEA, DEN, DRCP, F-30207 Bagnols sur Cèze

(3) Université Nice Sophia Antipolis, Institut de Chimie de Nice, UMR7272, 06108 Nice, France

Abstract

In case of an accidental nuclear event, contamination of humans by actinide elements may occur. Such elements have the particularity to exhibit both a radiological and chemical toxicity that may induce severe damages at several levels depending on the bio kinetics of the element. In order to eliminate the actinide elements before they are stored in target organs (depending on the element: liver, kidneys, bone), sequestering agents must be quickly injected. However to date, there is still no ideal sequestering agent, despite the recent interests in contamination concerns. DTPA (diethylenetriaminepentaacetic acid) raises current interests for an oral or alternative self-administrable form. Although mostly biokinetics data are available, molecular scale characterization of the actinide-DTPA complexes is still scarce. Nevertheless, a strong interest is arising for the characterization of $An^{IV}DTPA^{-}$ complexes at the molecular level because it opens the way for predicting stability constants of unknown systems or even for developping new analytical strategies aimed at better and more selective decorporation. For that purpose, investigations by Extended X-ray Absorption Fine Structure (EXAFS) and Ab Initio Molecular Dynamics (AIMD) were undertaken and compared with capillary electrophoresis (CE) used in a very unusual way. Indeed, the incapability of CE to extract structural information is commonly admitted. In capillary electrophoresis the electrophoretic mobility of an ion is a function of its charge and size. Despite very similar $\frac{z}{r}$ ratios, partial separations between $An^{IV}DTPA^{-}$ species (An^{IV} = Th, U, Np, Pu) were obtained. A linear relationship between the electrophoretic mobility and the distance actinide – oxygen calculated by AIMD was evidenced. As example, the interpolated distances U-O in $U^{IV}DTPA^{-}$ from CE-ICPMS experiments, EXAFS, AIMD and relation between the stability constants and the ratio $z/d_{An\text{-}O}$ agree all together. It results in the capability to evaluate the stability constants for the formation of $Pa^{IV}DTPA^{-}$, $Am^{IV}DTPA^{-}$ or $Bk^{IV}DTPA^{-}$.

Introduction

Diethylenetriaminepentaacetic acid (DTPA) is a polyaminocarboxylic acid of great interest in biochemistry and in the industry. For instance, DTPA calcium salt is usually applied as decorporating agent of actinides in case of contamination. It is also an essential reagent in actual and future nuclear spent fuel reprocessing processes (TALSPEAK process for the separation actinide/lanthanide in USA [1], and SANEX-TODGA process for the actinide/fission products separation in France). In the case of the ligand usually recommended for removing actinide from the human body, the constraints related to the complexity of DTPA (polydenticity, several types of donor atoms, large number of atoms) and that of the chemistry of actinides in solution (especially the plutonium ion) refrained from accessing extensive data in solution chemistry and in coordination chemistry. It is surprising that the affinity constants reported in the literature for the tetravalent actinides with DTPA are scarce, impeding to emphasize any useful trend. It is almost impossible to find a complete set of data even to date, from Th to Pu, using the same technique under the same operating conditions. Only one study fulfills these conditions: the technique applied was potentiometry in 0.5 M NaCl [2-5]. Unfortunately, the ionic strength does not match with biological medium and no further study has been carried out to confirm these results. There is a strong interest still in exploring the actinide series at the same oxidation state because the chemical properties of any of the elements can be predicted, particularly when an element is not detected due to a lack of sensitivity. For that purpose, a universal technique is mandatory providing that a) all elements respond in a similar manner and b) all elements can be detected simultaneously for a direct comparison under the same experimental conditions. Unfortunately, all the techniques applied up today do not satisfy both criteria. For instance, the spectrophotometry is used for U^{IV}-, Np^{IV}- and $Pu^{IV}DTPA^{-}$ [6-8] but not for Th^{IV} which is non UV-Vis absorbent. For the latter, only potentiometry [5, 6, 9] or ion exchange techniques [10, 11] have been used. Potentiometry had been really applied for the four actinides [2-5] but due to the inherent lack of selectivity of this technique, the experiments have been carried out with one element at a time. Due to the afore-mentioned difficulties, complete set of data can only be obtained by gathering data at I = 0.5 and 1.0 M from different techniques element by element. It results in a large scattering of available data and the impossibility to emphasize any reliable trend. As examples, variation up to 3 orders of magnitude is observed for the same element at I = 1.0 M: from 28.8 [12] to 31.8 [6] for $U^{IV}DTPA^{-}$, from 30.3 [7] to 32.3 [6] for $Np^{IV}DTPA^{-}$ and from 31.4 [8] to 33.67 [6] for $Pu^{IV}DTPA^{-}$.

As mentioned above, the need for data at low ionic strength (0.1 M) is crucial since in biological fluids; the ionic strength does not exceed 0.1-0.2 M (0.15 M in blood). It is surprising to note that at low ionic strength only data related to the formation of $Th^{IV}DTPA^{-}$ species are available. Likewise, the same discrepancy is noticed since *log* K largely varies between publications: 26.39 by spectrophotometry [13], 28.78 by potentiometry, and 30.34 by ion exchange [11]. These differences are too large for properly assessing the behavior of tetravalent actinides in blood. It is therefore crucial to refine data either by determining brand new and more precise values or to accurately evaluate them with an appropriate model. The first point must include the capability of jointly evaluating all data with a high degree of precision. The second one requires structural characterization and ab initio calculation to achieve an accurate model able to predict, with a high degree of confidence, any unknown chemical systems. It is the key point since in biological medium the metal ion interacts with many competing ligands (peptides, proteins) which could impede the metal sequestration by the decorporating reagent.

In this context, Capillary Electrophoresis coupled with an Inductively Coupled Plasma Mass Spectrometer (CE-ICPMS) gains a strong interest. Besides the capability to simultaneously detect all

metal ions, CE-ICPMS presents other advantages such as a very high sensitivity enabling to work at ultra-trace level (below 10^{-10} M) for all actinides and the capability to separate species without altering the initial speciation. The first point takes advantage in considering both no consumption of the ligand within a wide range of concentration (typically between 10^{-7} to 10^{-2} M) and the absence of polymeric species. The second point involves a non-intrusive physical process for achieving separation. Indeed, the separation by capillary electrophoresis is based on the difference of ion velocity when an electric field is applied at the extremities of the capillary. The speciation is not altered if the concentration of the ligand is constant at any time and any place in the capillary. This condition is easily achieved if both sample and electrolyte vials contain the same concentration of ligand.

The complexation of the tetravalent actinides by DTPA ligand involves a 1:1 limiting complex of very similar expected velocity since both size and charge are quasi identical. The stability of aqueous complexes should generally increase with respect to the charge-over-size ratio assuming an ionic model of the bonding [14]. Therefore a decrease of the metal-ligand distance is expected as both the effective charge grows and the ionic radius decreases. This induces small variations of size and subsequent small size variation of the hydrated species. However, the complete separation of all $An^{IV}DTPA^{-}$ species by capillary electrophoresis is not guarantee and there is a very high probability that the bands of migration overlap. In this framework, it is important to evaluate the mutual interactions and the potential effect upon the migration time. On the other hand, there are only a few studies showing the crystal structure of metal(IV) compounds with the ligand DTPA [15-17]. In the case of actinides, no reference appears to exist to date. Cristallochemical structure of Sn(IV), Hf(IV) and Zr(IV) complexes show that the coordination number (CN) is 8. However for Hf(IV), the CN may vary between 8 and 9 [16] and this seems to be linked to the existence in solution of the two complexes in equilibrium [17].

This paper will focus on the capability for CE-ICPMS to detect small variations of electrophoretic mobility in case of peak overlap. Nonetheless, in order to relate the electrophoretic data to direct structural information, complementary tools will be also employed. On the one hand, the combination of a local structural probe with theoretical tools is a unique opportunity to unravel the molecular speciation of these complexes in a way that has never been addressed in the related literature. EXAFS is a local structural probe that is ideally suited for complexes in solution because it is independent of the physical state of the system. At the actinide edge, it will allow to describe the cation coordination sphere, as already exemplified for the nitrilotriacetic ligand [18]. On the other hand, *ab initio* molecular dynamics could shed some light on the structure of complexes and will allow describing trends in the series $An^{IV}DTPA^{-}$ (from Th to Bk). Quantum molecular dynamics simulations – ABINIT code – will be carried out and compared with experiments (EXAFS, CE-ICPMS).

Theoretical

In capillary electrophoresis, the motion of ions is described by the Onsager and Fuoss treatment of conductance in mixed electrolytes [19]:

$$\mu(I) = \mu_0 - \left(\frac{e^3}{12\pi} \sqrt{\frac{N_{AV}}{(\varepsilon k T)^3}} \cdot z \cdot \mu_0 \sum_{n=0}^{\infty} C_n R^{(n)} + \frac{e^2}{6\pi\eta} \sqrt{\frac{N_{AV}}{\varepsilon k T}} |z| \right) \frac{\sqrt{I}}{1 + \frac{Ba}{\sqrt{2}}\sqrt{I}} \quad (1)$$

e is the elementary charge, N_{AV} is the Avogadro constant, ε is the permittivity of the solution, η is the viscosity of the solution, k is the Boltzmann constant, T is the temperature, $R^{(n)}$ is the nth component of a vector **R** and C_n is the nth member of a series [19] which is calculated by the formula $C_n = \frac{\prod_{i=0}^{n-1}(p-i)}{n!} \times \frac{-\sqrt{2}}{2}$ with $C_0 = \frac{1}{2}\left(2 - \sqrt{2}\right)$ and p = ½, a is the diameter of the ion. $\frac{Ba}{\sqrt{2}}$ is a free parameter generally taken to 1.5 [20]. The vector $R^{(n)}$ is determined by a recursion formula [19]:

$$r_j^{(n)} = (2H - 1)_{ji} r_i^{(n-1)};\ r_j^{(0)} = r_j \quad (2)$$

with h_{ji} the component of the matrix **H** calculated by the formula:

$$h_{ji} = \delta_{ji} \sum_i \phi_i \frac{\omega_i}{\omega_i + \omega_j} + \phi_i \frac{\omega_i}{\omega_i + \omega_j}, \quad (3)$$

δ_{ji} = 1 for $i = j$ and 0 otherwise, $\omega_i = \frac{\lambda_i^0}{\lambda_i^0 + \lambda_j^0}$, ϕ_i is the ionic fraction expressed in concentration. In practice, only the first five terms of the series C_n (n = 5) will be calculated because they already give four figures accuracy [19].

The first member in Eq.(1) describes the relaxation effect (electrostatic correction) and the second one the electrophoretic effect (hydrodynamic correction). In particular, by neglecting the medium effect (background electrolyte) common for all ions under motion, the presence of other $An^{IV}DTPA^-$ co-ions modifies the magnitude of the relaxation (term $\sum_{n=0}^{\infty} C_n R^{(n)}$). It could lead to an apparent separation between species due to relaxation but not due to size variation. In practice, we arbitrarily chose $Th^{IV}DTPA^-$ as target species and $Np^{IV}DTPA^-$ and $Pu^{IV}DTPA^-$ as co-ions. The electrophoretic mobility $\mu_{Th^{IV}DTPA^-}$ is calculated for increasing concentrations of the two 2 co-ions between 10^{-10} to 10^{-2} M. This variation depicted in the Figure 1 has gathered 100 pairs of ([$Np^{IV}DTPA^-$], [$Pu^{IV}DTPA^-$]) concentration values. The electrophoretic mobilities have been obtained from experiment at pH 6 where the three actinides had been simultaneously injected in the capillary. The mutual effect appears above 10^{-4} M and quickly increases when the concentration of all co-ions is higher than one millimolar. The magnitude of this effect is extremely small but it can induce a significant shift of the migration time. Thus, according to the Figure 1, the difference of migration times depicted in the Figure 2 between $Th^{IV}DTPA^-$ and $Np^{IV}DTPA^-$ (Δt = 0.6 s) could also be induced hypothetically by co-ions concentrations of about 0.01 M. Therefore, the individual mobilities can be considered as not correlated if the co-ions concentration is below 10^{-4} M. At the concentration used in our experiments (10^{-7} M) this effect will be ignored.

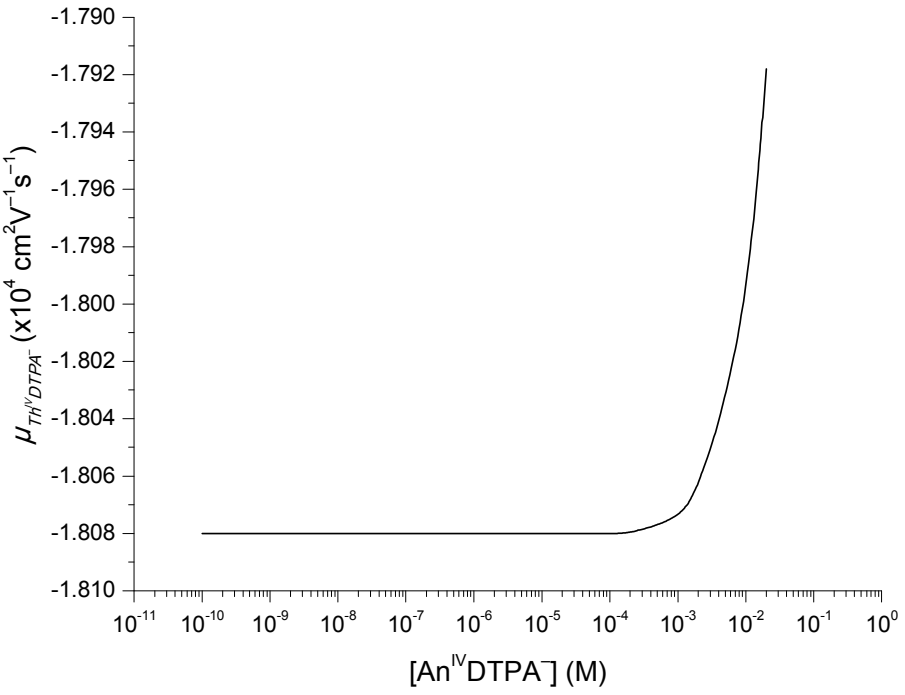

Figure 1 : variation of the $Th^{IV}DTPA^-$ electrophoretic mobility as a function of the total concentration of $An^{IV}DTPA^-$ co-ions (An=Np + Pu). Input parameters: $\mu_{Th^{IV}DTPA^-}$ = −1.808 10^{-4} $cm^2V^{-1}s^{-1}$, $\mu_{Np^{IV}DTPA^-}$ = −1.815 10^{-4} $cm^2V^{-1}s^{-1}$, and $\mu_{Pu^{IV}DTPA^-}$ = −1.817 10^{-4} $cm^2V^{-1}s^{-1}$, *I* = 0.1 M $NaClO_4$, T = 25 °C, [$Th^{IV}DTPA^-$] = 5 10^{-7} M, [$An^{IV}DTPA^-$] = from 10^{-10} to 10^{-2} M, [H^+] = 3.14 10^{-7} M. Viscosity and permittivity of sodium perchlorate solution are taken from the literature [21, 22].

Experimental

CE-ICPMS. A commercial Beckman Coulter P/ACE MDQ capillary electrophoresis system (Fullerton, USA) equipped with a UV detection mode was used for all separations in the same conditions that have been previously described (fused silica, 50 µm internal diameter, ~60 cm length, 10.1 cm optical window) [23]. An Axiom (VG Elemental, Winsford, Cheshire, U.K.) inductively coupled plasma sector field mass spectrometer (ICP-SF-MS) was coupled with the capillary electrophoresis using a commercial interface (Mira Mist CE, Burgener, Mississauga, Canada). A makeup liquid is introduced thanks to a syringe pump (11 Pico Plus, Harvard Apparatus, Holliston, MA) at a nominal flow rate of 6 µL.min^{-1}. Separations were performed at +10 kV, 25 °C and at a constant pressure of 0.5 psi (to avoid capillary clogging). The voltage value was chosen with respect to the Ohm law and to avoid for any experiment a temperature rise superior to 1 °C. The buffer vial was changed every run to avoid the effects of electrolysis. Before each run, the capillary was washed with the background electrolyte (BGE) for 10 min at 20 psi and 2 min at 40 psi. Sample injections were hydrodynamically carried out at 0.5 psi for 3 s.

BGE were prepared from weighted amounts of $NaClO_4$, DTPA (diethylenetriaminepentaacetic acid, Sigma 99 %) and MES (low moisture content, Sigma 99%) dissolved in Millipore deionised water (Alpha-Q, 18.2 MΩcm). The final solution contains DTPA at 10^{-2} M or 10^{-4} M, MES at 2 10^{-2} M. Several solutions have been prepared at various pH: pH 5.0, 6.0 and 6.5 and 7.0 by adding suitable amount of NaOH in the BGE. The ionic strength is adjusted to 0.1 M by $NaClO_4$.

Sample preparation: The Th^{IV} stock solution was prepared by dissolving thorium nitrate ($Th(NO_3)_4,5H_2O$) in nitric acid solution. The U^{IV} solution (1.1 M HNO_3, 0.15 M $N_2H_5^+$) was prepared by catalytic reduction of U^{VI}, and then was stabilized by hydrazinium nitrate solution. This solution is diluted to obtain a 4.8 10^{-2} M U^{IV} stock solution in 0.5 M HNO_3. The Np^{IV} solution was prepared by reducing 5 10^{-2} M Np^{V} in 0.5 M HCl with 0.5 M hydroxylamonium chloride at 70 °C during a few days. The resulting stock solution is stable over several months. The Pu^{IV} solution was prepared by the purification in an anionic ion exchanger (Dowex, AGMP1). The eluate is diluted to get a final concentration of 3.15 10^{-2} M in 0.95 M HNO_3 solution.

All samples were prepared by diluting the appropriate volume of Th^{IV}, U^{IV}, Np^{IV}, and Pu^{IV} stock solutions into the BGE. Dimethylformamide (DMF) was added (0.2 µL) in the samples before the analysis in order to determine the magnitude of the electroosmotic flow (eof).The concentrations were 10^{-7} M for all tetravalent actinides.

EXAFS experiments. EXAFS measurements were performed in 200 µL cells specifically designed for radioactive samples at room temperature. EXAFS data have been recorded at both SSRL (Stanford Synchrotron Radiation Laboratory, Stanford, USA) and ESRF (European Synchrotron Radiation Facility, Grenoble, France) synchrotrons on 11-2 and BM20 beamlines respectively. All spectra were acquired at the actinide L_{III} edge. The 11-2 beam line (Th, Np) is equipped with a liquid nitrogen cooled double crystal Si(220) monochromator and with two collimating and focusing rhodium coated mirrors. A 30-element Ge solid state detector was used for data collection in the fluorescence mode. The BM20 beam line (Pu) is equiped with a Si(111) water cooled monochromator in the channel cut mode. Two Pt coated mirrors were used for harmonic rejection. Data were collected in transmission mode with gas filled ionization chambers. In all cases, the monochromator enery calibration was performed with a Y foil (17052 eV at the absorption maximum) and Zr foil (18014 eV at the absorption maximum) depending of the actinide cation edge.

Data processing was carried out using the ATHENA code [24]. The *e0* threshold energy was identified at the maximum of the absorption edge. Fourier Transformation (FT) in k^2 was performed between 2.5 and 10.5 $Å^{-1}$ with Hanning windows using the ARTEMIS code [24]. With this spectral range, the number of independent points is equal to 18.

The $Pu^{IV}DTPA^-$ model obtained with theoretical calculations (see the ab initio calculation section) was used for the calculation of the phases and amplitudes of each scattering path using Feff84 code [25]. Multi-shell adjustment of the experimental EXAFS data was carried out with ARTEMIS code in R space between 1 and 5 Å. Two independent single scattering paths, An-O (5 degenerate) and An-N (3 degenerate) were included for the first coordination sphere. For the second coordination sphere, the following paths were included : one single scattering path, An---$C_{\alpha(O)}$ (where "---" accounts for no chemical bond), accounting for the $C_{\alpha(O)}$ atoms of the carboxylate (5 degenerate); one single scattering path, An---$C_{\alpha(N)}$ accounting for the $C_{\alpha(N)}$ atoms of the amine functions (9 degenerate); one triple scattering path An---$C_{\alpha(O)}$-O of the carboxylate (10 degenerate). Both An---C single scattering paths were linked with the corresponding An-O and An-N distances (with geometrical relations). The triple scattering path was also linked to the corresponding An-O path the same way. Finally for the third coordination shell, an independent triple scattering path An---C-O accounting for the distal O atom of the carboxylate was included (10 degenerate).

Ab initio calculations. *Ab initio* molecular dynamics (AIMD) is a powerful simulation technique for calculating structural and physical properties of matter. High parallel computing facilities now allow studying such systems as DTPA complexes. In the framework of DFT-PAW formalism (Density Functional Theory-Projector Augmented Wave) we used the ABINIT code [26] for performing AIMD simulations on $An^{IV}DTPA^{-}$, An=Th, U, Np, Pu, Am, Bk. Although $Am^{IV}DTPA^{-}$ and $Bk^{IV}DTPA^{-}$ don't exist due to the oxidation of DTPA by M(IV) according to the high potential M(IV)/M(III), the calculation of the whole series present a fundamental interest with application to other solvents (e.g. ionic liquids).

For each case, we have treated an isolated charged complex in a large simulation box in order to simulate the gaseous phase. The cell size has to be large enough to neglect the interactions between the periodic images. Moreover in charged systems, the strong and long-range Coulomb interaction between the localized charge distributions converges very slowly. The most common approaches consist in fixing a rather large simulation cell (45 Bohr) and correcting *a posteriori* the finite-size cell errors in the total energies [27]. The simulations are run in the isokinetic ensemble at 298 K until equilibration is achieved, i.e. until the variations in pressure stabilize to an oscillatory pattern, without any long-term trend. Following equilibration, the pressure and energy are calculated by averaging over the next 4000 time steps of 0.48 fs each. All calculations have been done at the Γ point, the center of the Brillouin zone. For each element a PAW data set have been fixed and a pseudo-potential built [28]. The data were generated for the Perdew-Burke-Ernzerhof (PBE) exchange-correlation functional with relativistic corrections to the wave function [29]. We have chosen a standard actinide basis set with 7s, 6p, 6d, 5f in the valence band and 6s and 6p as the semicore orbitals. The validity of pseudo-potentials was checked by performing and comparing calculations on actinide metals and oxides – cell parameter and bulk moduli – to all electrons calculations. In ABINIT the energy cut off is an important parameter and we investigated the convergence needed for obtaining reliable results.

In heavy actinides systems, the presence of correlated *5f* electrons leads to an improper description of the electronic and the structural properties by density functional theory. Several approaches have been developed to overcome these shortcomings of DFT and the DFT+U (Local Density Approximation LDA+U or Generalized Gradients Approximation GGA+U) approach has been shown to effectively correct many deficiencies. Subsequently, except for thorium (no *5f* electron in Th^{IV}), we introduce Hubbard U and Hund's J parameters for the onsite interaction strength. Although the choice of U and J are debatable we used the same values for U, Np, Pu, Am and Bk *i.e.* the classical values obtained for tetravalent plutonium oxide (U=4 eV, J=0.2 eV) [30]. Apart from Th^{IV} ($5f^{0}$) and Bk^{IV} (half-filled $5f^{7}$), in order to avoid metastable states, the electron-electron interaction potential was fixed in the Hamiltonian according to a given occupancy matrix n_{ij}^{σ}, for the *5f* correlated states during the first eight steps of the energy minimization procedure. It was then self-consistently optimized.

Results

EC.ICPMS. According to the ionic model of chemical bonding (chemical forces are largely of electrostatic type), the bond energy between is governed by the size and charge of the reactant. In the particular case where the same ligand is studied with various metal (e.g. tetravalent actinides), it

is expected a relationship in $\frac{z_M}{d_{M-L}}$, where z_M is the effective charge of the metal and d_{M-L} the bond distance between the metal M and the ligand L [14]. A similar relation exists in the ion transport theories by coupling the Stoke-Einstein diffusion law with the definition of the electrophoretic mobility [31]:

$$\mu_{M-L} = \frac{z_{M-L}e}{6\pi\eta r_{M-L}}, \quad (4)$$

where $z_{M\text{-}L}$ is the charge of the complex M-L, $r_{M\text{-}L}$ the ionic radius of the hydrated complex M-L.

Both relations involve a dependence of charge and size. For a same charge of the complex, it is then expected an effect of $d_{M\text{-}L}$ (because of concomitant r_{M-L} variation) on the electrophoretic mobility μ_{M-L}. The electrophoretic mobility (μ_{M-L}) is experimentally determined by subtracting the osmotic mobility (μ_{eo}) measured with DMF to the actinide apparent mobility (μ_{app}):

$$\mu_{M-L} = \mu_{app} - \mu_{eo} = \frac{L^2}{V}\left(\frac{1}{t_{M-L}} - \frac{1}{t_{eo}}\right) \quad (5)$$

with L the capillary total length (cm), V the applied voltage (V), t_{M-L} the migration time of actinides complex (s) and t_{eo} the migration time of DMF (s).

In order to compare the same type of complexes, the conditions of separation must be properly chosen in such a way the complex $An^{IV}DTPA^-$ is the unique species in solution for all actinides. Whatever the stability constant values taken for calculating the speciation diagram (see Table 1), $An^{IV}DTPA^-$ is the unique species present in solution for [DTPA] = 10^{-4} to 10^{-2} M. Although the existence of hydroxo-DTPA-metal complex has been reported for U^{IV} [32] ($log\ K$ = 7.69 ± 0.02 ; $UL^- + H_2O \rightleftharpoons ULOH^{2-} + H^+$) and Th^{IV} [33] ($log\ K$ = 8.9 ; $ThL^- + H_2O \rightleftharpoons ThLOH^{2-} + H^+$), these species are negligible under our experimental conditions (5 < pH < 6.5).

Table 1: Bibliography of stability constants related to the formation of $An^{IV}DTPA^-$ at 20 °C (*I* = 0.1 & 0.5 M) and 25 °C (*I* = 1.0 M).

Actinide	I = 0.1 M	I = 0.5 M	I = 1.0 M
Th^{4+}	28.78 ± 0.10 [9] 30.34 ± 0.03 [11] 26.39 [13]	26.64 ± 0.03 [2]	29.6 ± 1.0 [6] 26.6 [12]
U^{4+}	30.9 [34]	28.76 ± 0.09 [3]	31.8 ± 0.1 [6] 28.8 [12] 29.9 [8]
Np^{4+}		29.29 ± 0.02 [4]	30.5 [8] 32.3 ± 0.1 [6] 30.96 [10] 30.33 ± 0.12 [7] 30.3 [12]
Pu^{4+}		29.49 ± 0.10 [5]	31.4 [8] 33.67 ± 0.02 [6] 29.5 [12]

An example of the separation of $An^{IV}DTPA^-$ species is depicted in the Figure 2. Their detection by CE-ICPMS has always shown one peak which results in a fast equilibrium between the formation and the

dissociation of the complex [35, 36]. As expected, their migration times are close (but not identical) due to similar charge and size. It is qualitatively observed in all experiments the order of migration $\mu_{Pu^{IV}DTPA^-} > \mu_{Np^{IV}DTPA^-} > \mu_{Th^{IV}DTPA^-}$ which follows the decrease of the ionic radius along the tetravalent actinide series: $r_{\mathrm{Pu}} < r_{\mathrm{Np}} < r_{\mathrm{Th}}$.

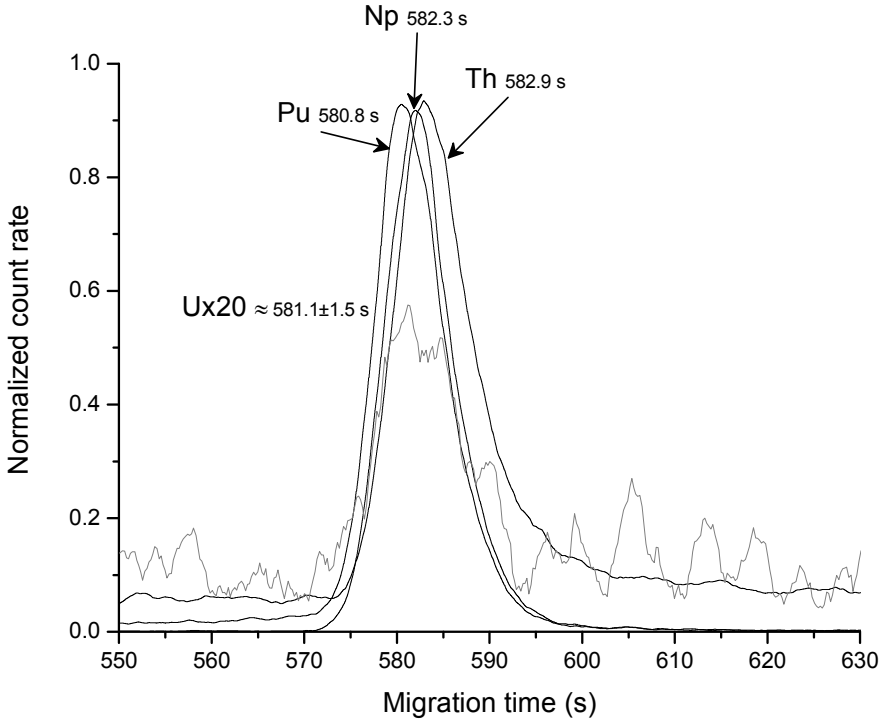

Figure 2 : Electropherograms of $An^{IV}DTPA^-$ species. Conditions of separation: [DTPA] = 10^{-2} M, [An^{4+}] = 10^{-7} M, electrolyte support 0.1 M $NaClO_4$, pH 6.045, V = 10 kV, L = 59.6 cm, T = 25 °C, injection 0.5 psi for 3 s. The signal relative to the U^{IV} has been increased by a factor of 20. The electropherograms have been smoothed (20 points) in order to minimize the fluctuations appearing in the "time slice" mode of ICPMS (each mass, 232, 237, 238, and 239 is successively counting during 10 ms).

According to the Equation 1, the electrophoretic mobility is strongly dependent on the temperature and the ionic strength and cannot be exactly and precisely kept identical from one experiment to another one. In order to minimize the unavoidable fluctuations between samples, all electrophoretic mobilities have been calculated relative to that of thorium (Table 2). However, although minimized, such effects mainly contribute in the accuracy and the repeatability and lead to an overall uncertainty of about 5-10 %.

The difference of mobility is small but enough precise to systematically observe the same order: $\mu_{Pu^{IV}DTPA^-} > \mu_{Np^{IV}DTPA^-} > \mu_{Th^{IV}DTPA^-}$.

Table 2: relative mobility of An^{IV} (An^{IV} = U, Np, Pu) as function of pH and ionic strength. The electrophoretic mobility of $Th^{IV}DTPA^-$ is taken as reference.

$\Delta\mu = \mu_{An^{IV}DTPA^-} - \mu_{Th^{IV}DTPA^-}$ ($cm^2V^{-1}s^{-1}$)	An = U^{IV}	An = Np^{IV}	An = Pu^{IV}
pH = 5.05, I = 0.05 M	–	–0.0862	–0.0953
pH = 5.98, I = 0.05 M	–0.0665	–0.0921	–0.0909

pH = 6.05, I = 0.1 M	–0.0171	–0.0166	–0.0268
pH = 6.07, I = 0.05 M	–	–0.0919	–0.1021
pH = 6.45, I = 0.05 M	–	–0.0749	–0.0996
pH = 6.50, I = 0.1 M	–	–0.0315	–0.0431

EXAFS results. EXAFS data have been recorded for the 1:1 $An^{IV}DTPA^{-}$ (An = Th, Np, Pu) complexes in acidic perchloric solutions. The spectrum of $U^{IV}DTPA^{-}$ has not been recorded because it was technically difficult at this stage to stabilize U(IV) against oxidation throughout the experiment. The EXAFS signals shown in Figure 3 are all very similar and their corresponding Fourier transforms (FT) exhibit a first major contribution between *ca* $R + \Phi$ = 1 and 2 Å, a second complex contribution of smaller intensity centred around $R + \Phi$ = 2.6 Å and a third contribution of minor intensity centered around $R + \Phi$ = 2.9 Å. Qualitatively, these features may correspond to the bonding of An^{4+} by light atoms in the first coordination sphere and further backscattering from the backbone of the ligand (C, O atoms) in the second and third coordination spheres.

The quantitative adjustment of the EXAFS data has been performed based on the theoretical model defined by DFT calculations with a 5+3 coordination mode (see next section) in the first coordination sphere. Given the relatively large uncertainty associated to amplitude functions in the absence of experimental model compound (usually between 10 and 20 %), and because the EXAFS signal of the first shell is here exclusively dominated by light scattering atoms (O and N) of similar atomic numbers, the number of neighbours has not been refined and been kept constant (5O + 3N) and equal to the 5+3 model. This constraint precludes testing the occurrence of additional water molecules in the first coordination sphere of Th for instance. The putative addition of a water molecule for the ligther actinides as Th would fell in the error range of EXAFS amplitude determination (1 over 8 makes 12 %). In conclusion, fluctuation of ± 1 oxygen atom in the first coordination from Th to Pu is impossible to determine in these conditions with EXAFS. Another consequence of the backscattering similarity between the O and N atoms is that the concomitant presence of O and N in the first coordination sphere with distance splitting less than 0.6 – 0.7 Å (of the same order as the spectral resolution given by $2\pi/\Delta k$ = 0.78 Å) is difficult to assess. As expected from the above remarks, the Debye Waller factors reported in Table 3 and associated with the An-N path are relatively high (around 0.02 $Å^2$). In order to overcome this difficulty, one possibility is to take into account the second and third coordination spheres and perform a multi-shell parameterized fit. Given the structure of the 1:1 complex obtained from theoretical calculations, the second shell has been geometrically linked to the first one (see experimental section for details on the fitting procedure). Consequently, the An-N distances determined in the fit are largely driven by the second coordination sphere. Nevertheless they must be discussed with much care and are indeed associated with large error bars. A similar example of this type of O + N coordination has been reported for nitrilotriacetic acid [18], the smallest of the polyaminocarboxylate ligands. According to the parameters of Table 3, the An-O distances decrease from 2.40 Å for Th to 2.30 Å for Pu, again in agreement with the cation contraction. In all cases, the An-N distances stay significantly larger (between 0.3 and 0.4 Å) than the An-O distances and this is consistent with a first shell of the 5+3 model.

Table 3: EXAFS best fit parameters for the $An^{IV}DTPA^{-}$ (An = Th, Np, Pu) complexes in acidic perchloric solution. Numbers in italics have been fixed or linked. Coordination numbers have been fixed to the 5+3 model. Numbers in brackets are the

estimated uncertainties. σ^2 is the Debye Waller factor of the considered scattering path. S_0^2 is the global amplitude factor, $e0$ is the energy threshold, R_{factor} is the agreement factor of the fit in %.

Th(IV)	*5* O at 2.40(1) Å σ^2 = 0.0046 Å^2	*3* N at 2.71(10) Å σ^2 = 0.0291 Å^2	*5* C_α at *3.43* Å σ^2 = 0.0169 Å^2 *9* C_β at *3.50* Å σ^2 = *0.0169* Å^2	S_0^2 = 1.1 *e0* = –2.95 eV R_{factor} = 4.8%
Np(IV)	*5* O at 2.29(1) Å σ^2 = 0.0038 Å^2	*3* N at 2.60(3) Å σ^2 = 0.0234 Å^2	*5* C_α at *3.33* Å σ^2 = 0.0160 Å^2 *9* C_β at *3.40* Å σ^2 = *0.0160* Å^2	S_0^2 = 1.0 *e0* = –5.00 eV R_{factor} = 4.4%
Pu(IV)	*5* O at 2.30(1) Å σ^2 = 0.0049 Å^2	*3* N at 2.61(3) Å σ^2 = 0.0169 Å^2	*5* C_α at *3.34* Å σ^2 = 0.0126 Å^2 *9* C_β at *3.40* Å σ^2 = *0.0126*Å^2	S_0^2 = 1.0 *e0* = –5.27 eV R_{factor} = 4.2%

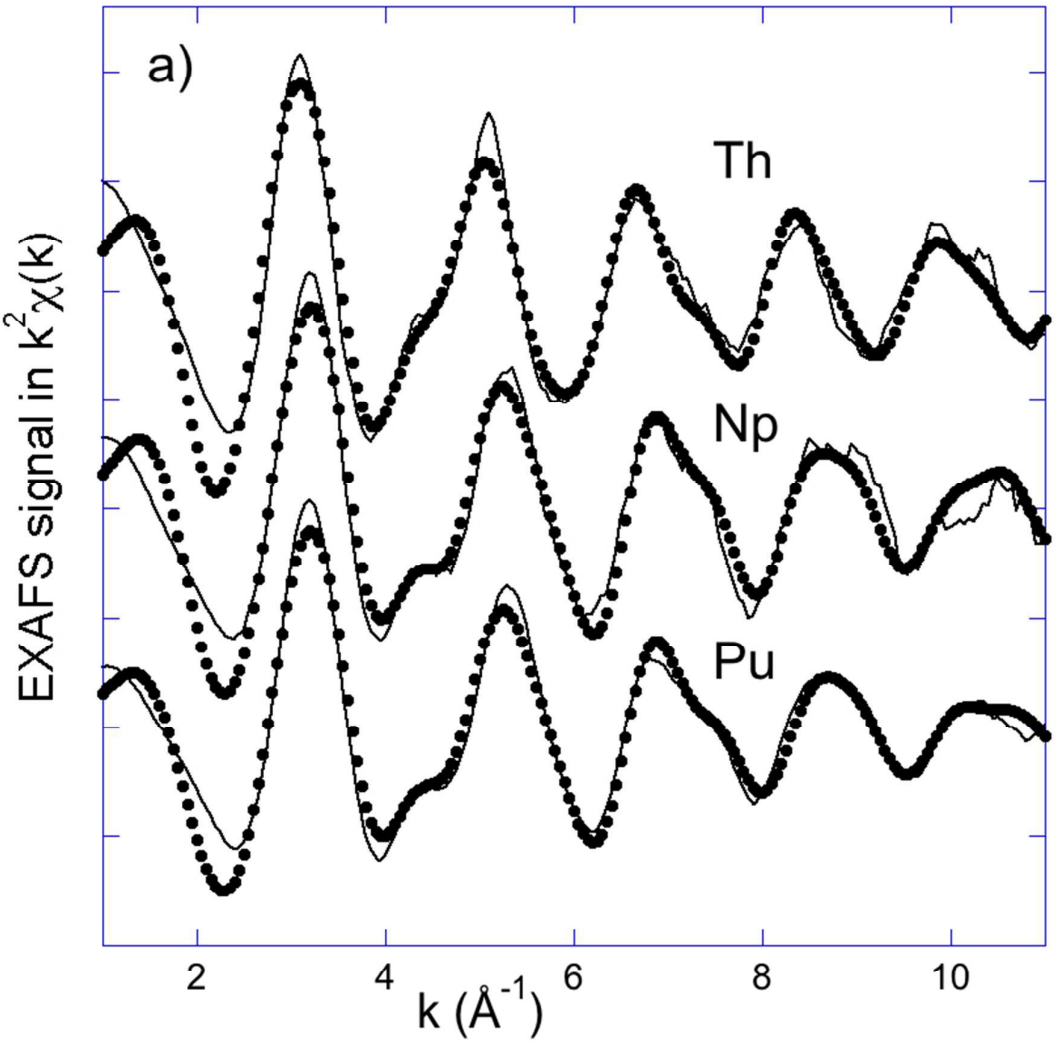

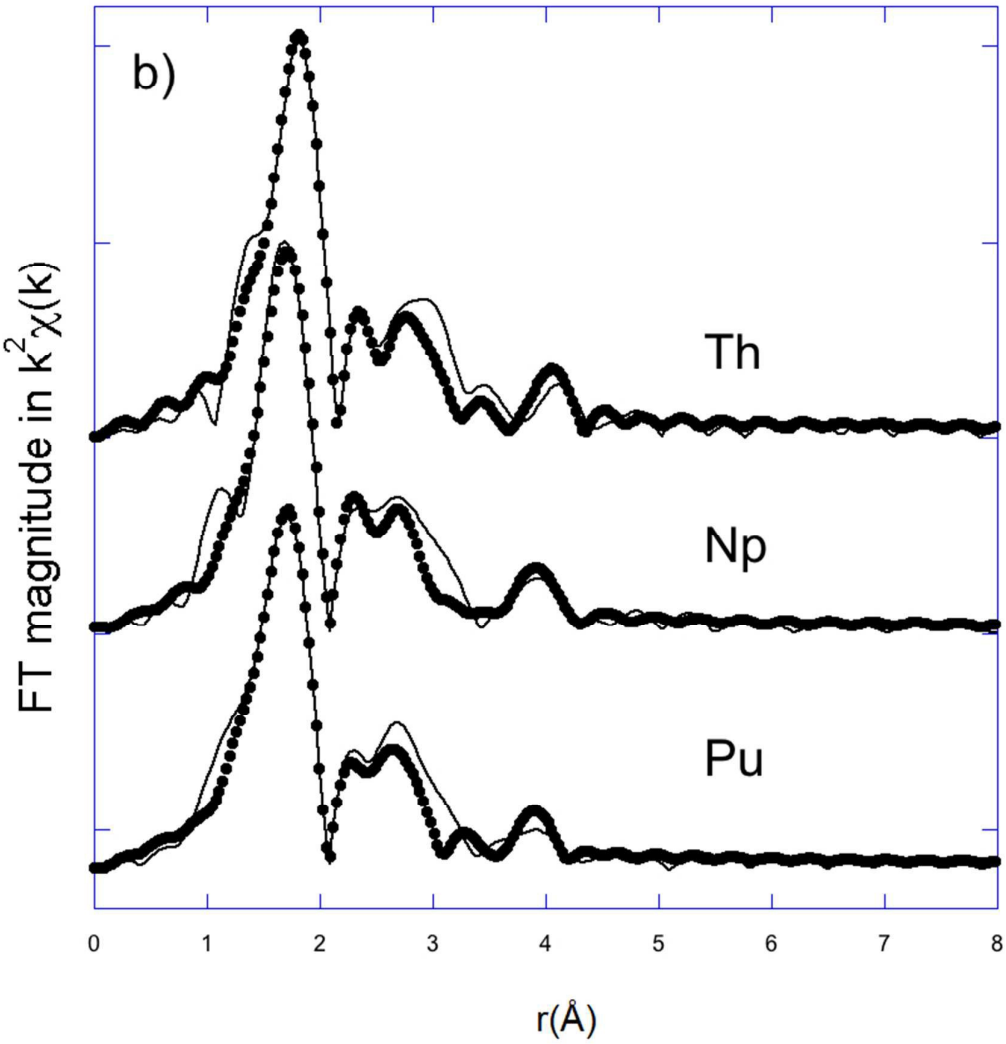

Figure 3 : a) EXAFS spectra of the $An^{IV}DTPA^{-}$ (An = Th, Np, Pu) complexes in acidic perchloric solution; b) corresponding Fourier transform of the EXAFS spectra in $k^2\chi(k)$. Solid line = experimental spectrum, dots = adjustment. Spectra have been shifted in ordinates for clarity.

DFT results. Starting with $Pu^{IV}DTPA^{-}$, the dynamics evidenced a very different structure between LDA (or GGA) and LSDA+U. In the LDA (GGA) case, Pu-O distances are too short and Pu-N distances too long in comparison with EXAFS measurements. The *5f* electrons hybridized to the *6d* ones are located at the Fermi level and took part in the chemical bonding properties. The spin polarization pushed the *5f* states away the Fermi level and leads to a full polarization of these states with an integer 4 μ_B magnetic moment on plutonium ions. This localization effect implies a decrease of the Pu-O bond covalence and an increase of the bond length. A rather similar effect was observed on delta-plutonium metal and some of its binary compounds [37, 38]. As discussed, independently on the real physical meaning of magnetism in Pu the introduction of magnetic ordering in calculations leads to major improvements in comparison to the standard nonmagnetic LDA or GGA results (equilibrium volume, bulk moduli, and formation energies). LSDA+U formalism strengthens the electron localization and leads to an excellent description of all the bond lengths compared to EXAFS

investigations. During all our simulations the magnetic moment remains the same indicating the additional electron - total charge equals minus one in $Pu^{IV}DTPA^{-}$ - stays delocalized in the DTPA ligand. Experimentally, in aqueous solution Pu^{IV} would probably be paramagnetic.

A ligand's rolling up the central cation Pu^{IV} (Figure 4) is evidenced. The partial distribution pair functions (Figure 5) lead to the cation coordination. Two kinds of Pu-O bonds with five bonds at 2.25 Å and five bonds at 4.45 Å are observed, one kind of Pu-N bond with three bonds at 2.67 Å, two kinds of Pu-C bonds with nine Pu-C bonds with C bonded to N at 3.55 Å and five bonds with C bonded to O at 3.31 Å. Then the first Pu^{IV} coordination shell owns five oxygen ions from carboxylates and three nitrogen atoms from the DTPA amine skeleton. The second Pu^{IV} coordination shell is formed by the fourteen carbon atoms. The first coordination sphere is a distorted polyhedron. Performing some more trials with one and two water molecules in the vicinity of Pu^{IV} it was not possible to fix any water molecule in this inner-sphere. Comparing this structure to the well-known $Gd^{III}DTPA^{-2}$ system [39], in $Pu^{IV}DTPA^{-}$ the cation is located at the cup-like DTPA surface with a shorter cation oxygen bond (2.394 Å) and a longer cation nitrogen bond (2.644 Å), Gd^{III} staying inside the cup with a water molecule. This may be explained by simply steric considerations and Pearson different hardness character of the two cations.

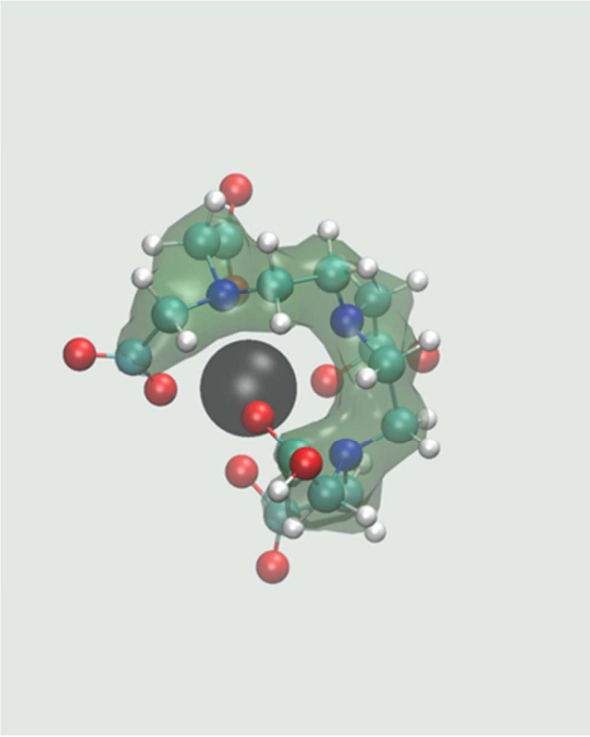

Figure 4: $Pu^{IV}DTPA^{-}$ calculated complex scheme. Oxygen atoms are in red, nitrogen in blue, carbon in cyan and hydrogen in white.

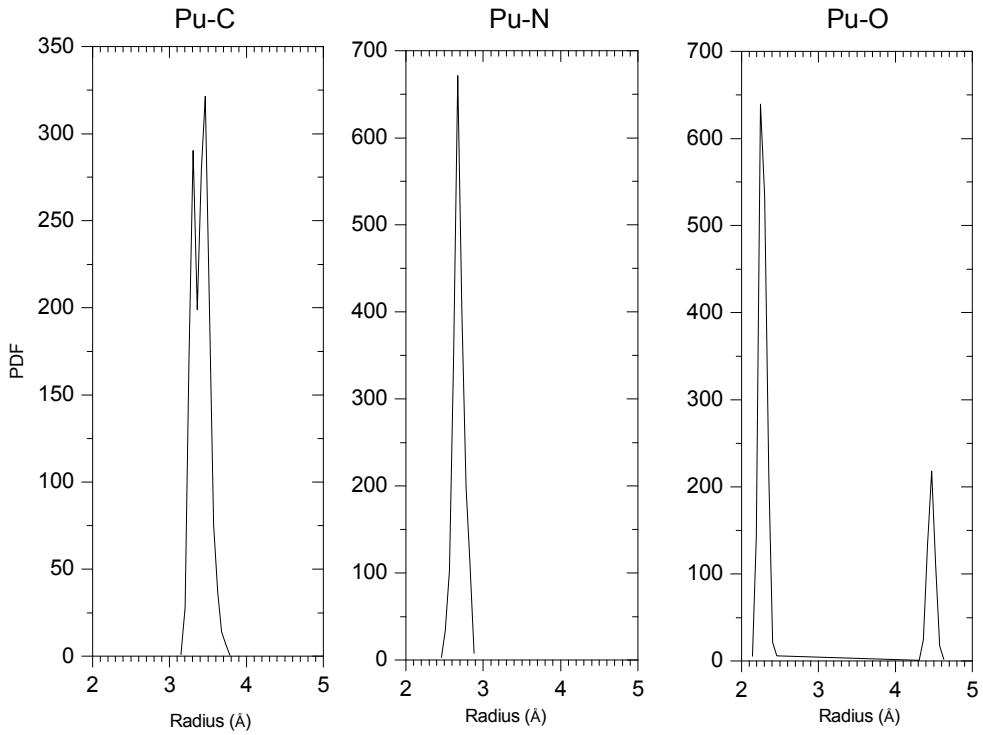

Figure 5 : Partial Pair Distribution Functions (PDF) in $Pu^{IV}DTPA^{-}$.

An-O and An-N distances are presented on Figure 6 for the series $An^{IV}DTPA^{-}$, An = Th, U, Np, Pu, Am and Bk. The An-O bond length decreases from Th to Pu and increases from Pu to Bk in agreement with EXAFS for the first part of the curve. The An-N bond length decreases along the series. According to the HSAB principle the bonding between the hard acid An^{IV} and the hard base O^{2-} is stronger than the bonding with the soft base N anion leading to a smaller bond length. The shape of An-O curve follows the shape of actinide volumes and electronic localization effect. In actinide metals the light actinides (Th to Pu) evidenced a decreasing volume like *5d* metals. Then the volume increases for the heavy actinides (Pu and beyond) like *4f* elements due to the strong localization of *5f* states. In a chemical picture the An cation acidic character softens from Th to Pu and hardens beyond.

The true systems only exist in aqueous solution and in order to check the effect of water, we performed a new dynamics for $Pu^{IV}DTPA^{-}$ surrounded by a solvation sphere of twenty water molecules. The same simulation conditions (298 K) as before have been used. After equilibration, we observed that the different bond lengths slightly changed compared to the isolated complex: Pu-O bonds increased from 2.25 Å to 2.30 Å, Pu-N bonds from 2.67 Å to 2.72 Å. The results get closer to EXAFS measurements respectively 2.30 Å and 2.61 Å. By Performing the same trial on $Th^{IV}DTPA^{-}$ we observed a water molecule located close to the thorium ion (Th-O (O of H_2O) bond at around 2.6 Å) in the first coordination shell. This water molecule stayed there during all the simulation time. These last results evidenced a change of the coordination number from 9 (Th) to 8 (Pu) along the actinide series. The nine-coordination mode observed for the complex $Th^{IV}DTPA(H_2O)^{-}$ agrees with the conclusion given by Fried and Martell based on IR and NMR spectra obtained in D_2O [40]. It is worth noting the effect of one water molecule does not significantly change the Th-O (O of DTPA) bond length.

Discussion

Distances O- and N-ligand-metal by AIMD and EXAFS.

EXAFS is a powerful technique for determining the bond lengths in the vicinity of the probed metal. However, this technique is not self-consistent and often requires structural assumptions supported theoretical parameters. In return, the ab initio simulation must be compared with EXAFS to check the validity of the model applied to describe the electronic configurations. Both techniques mutually feed but lead to their own values. Results are depicted in the Figure 6. The An-O distances obtained by EXAFS agree quite well with the calculations, as depicted in Figure 6a. But the An-N distances are significantly shorter than that obtained by theoretical calculations (around 0.2 Å). On the other hand, the second coordination An---C shell that is linked to the An-O and An-N distances is in fairly good agreement with the theoretical models (for instance for Pu: theoretical model = 3.31 Å, EXAFS = 3.38 Å). As explained in the previous section, these distances are only indicative and should be further considered with caution. For instance, a significant distortion of the DTPA backbone in comparison with the theoretical model may occur. Last, the fluctuations of the coordination number for the lighter actinides suggested by the theoretical calculations have not been considered by EXAFS.

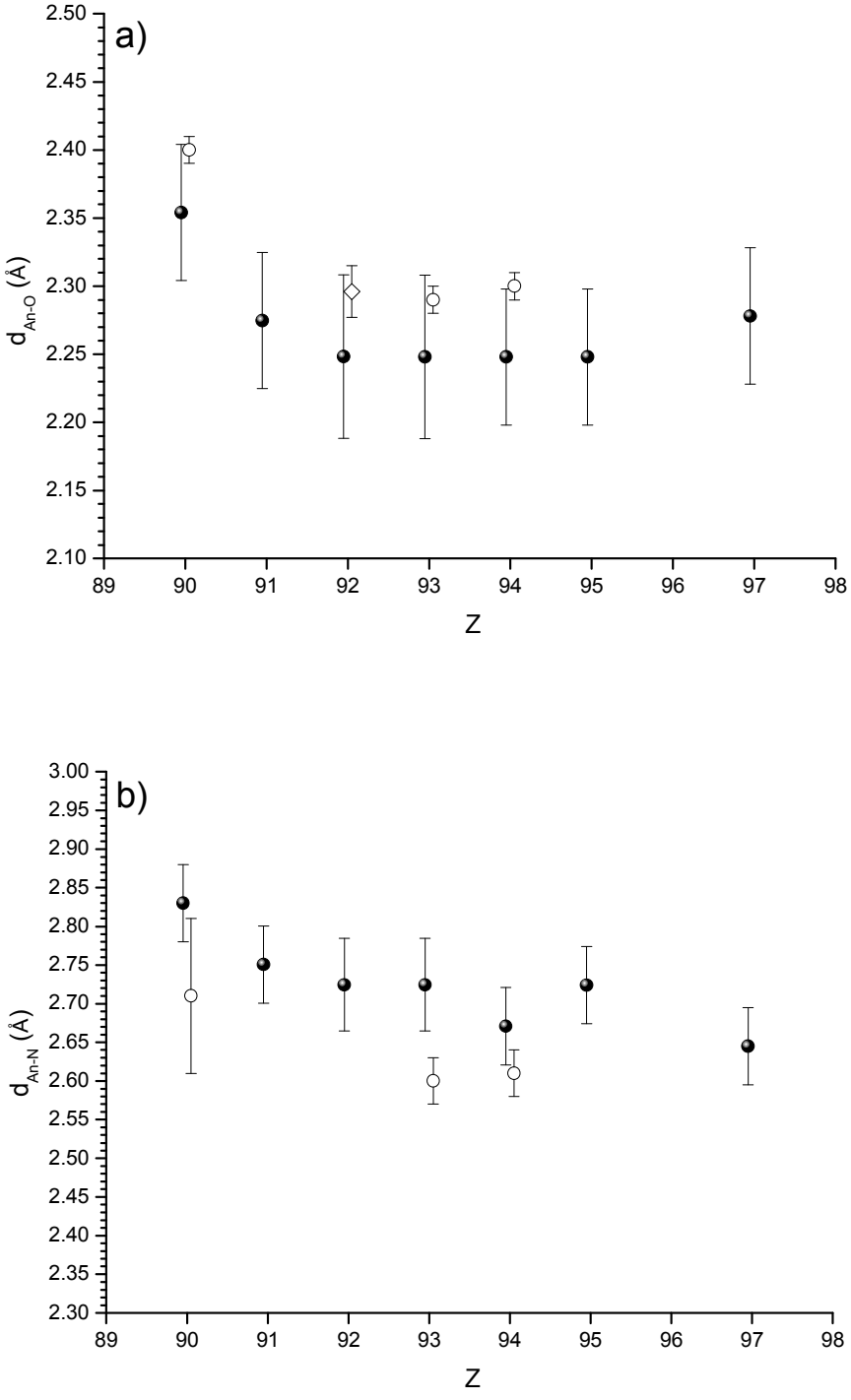

Figure 6: distances An^{IV}-oxygen (a) and An-nitrogen (b) by theoretical method (*Ab initio* molecular dynamics – AIMD) [●] and experiments (EXAFS [○], and average from thermodynamic+ CE values in Table 4 [◇]).

Relation stability constant – distance ligand-metal. The chemical system $An^{IV}DTPA^{-}$ has been studied for a long time but only a few sets of stability constants are available (see Table 1). The number of data is reduced when considering only the ionic strengths for which the stability constants are known for all the tetravalent actinides. In practice, only two sets of values at *I* = 0.5 M and *I* = 1.0 M are of interest. Due to the hardness character of tetravalent actinide a linear trend is expected between the stability constant and the distance oxygen-metal. We have reported in the Figure 7 the variation of $logK_{An^{IV}DTPA^{-}}$ (An = Th, U, Np, and Pu) as function of the ratio $z_{effective}/d_{An\text{-}O}$. Despite a nine-coordinated mode for Th, the distance $d_{An\text{-}O}$ is not significantly modified for $Th^{IV}DTPA^{-}$ complex. Data relative to other tetravalent ions (Zr and Hf) have been also reported when available. For the latter, the distances $d_{Metal\text{-}O}$ were obtained from X-ray diffraction [17] whereas thermodynamic data were taken from several sources [9, 41-45]. The stability constants were recalculated when necessary depending on the equilibrium found in the publications. Thus, DTPA acidity constants at I = 1.0 M [36] were used to determine the stability constant from the chemical equilibrium $M^{4+} + H_5DTPA \rightleftharpoons MDTPA^{-} + 5H^{+}$ to the chemical equilibrium $M^{4+} + DTPA^{5-} \rightleftharpoons MDTPA^{-}$ [41] whereas specific interactions coefficients $\varepsilon_{i,j}$ were used to calculate values from I = 0.23 [42] and 0.39 M [43] to 0.5 M. The following coefficients were chosen: $\varepsilon_{M^{4+},ClO_4^-} = 0.84$ [46], $\varepsilon_{Na^+,DTPA^{5-}} = 0.16$ [47] and $\varepsilon_{Na^+,MDTPA^-} \approx 0$ (estimate). The distances d_{An-O} were obtained by AIMD calculations for tetravalent actinides. In aqueous solution, the tetravalent actinides have an effective charge different from +4: +3.82 for Th^{4+}, +3.88 for U^{4+} and +3.97 for Np^{4+} and Pu^{4+}. Indeed, the electrostatic field of a highly charged ion affects the properties of water molecules in its vicinity. From EXAFS data, David and coworker developed a semi-empirical model in which the effective charge of lanthanide and actinide at the oxidation states III and IV was deduced from experimental distances metal-water molecules in the first hydration sphere [48]. For the smaller ions like Zr and Hf, the effective charge is +4.

In addition, the ionic radius decreases along the series from 1.05 for Th^{IV} to 0.96 Å for Pu^{IV} (CN = 8) [49]. From linear relation observed in the Figure 7, the distance U-O in the complex $U^{IV}DTPA^{-}$ can be evaluated by linear regression using Th, Np and Pu as input data and U as unknown parameter. U^{IV} is an interesting case because as redox sensitive cation, data is often missing (e.g. in CE, and EXAFS experiments). $z_{effective}/d_{An\text{-}O}$ is also adequately located as intermediary point between Th^{IV} and Pu^{IV}. The distances U^{IV}-O in $U^{IV}DTPA^{-}$ calculated for all techniques are gathered in the Table 4.

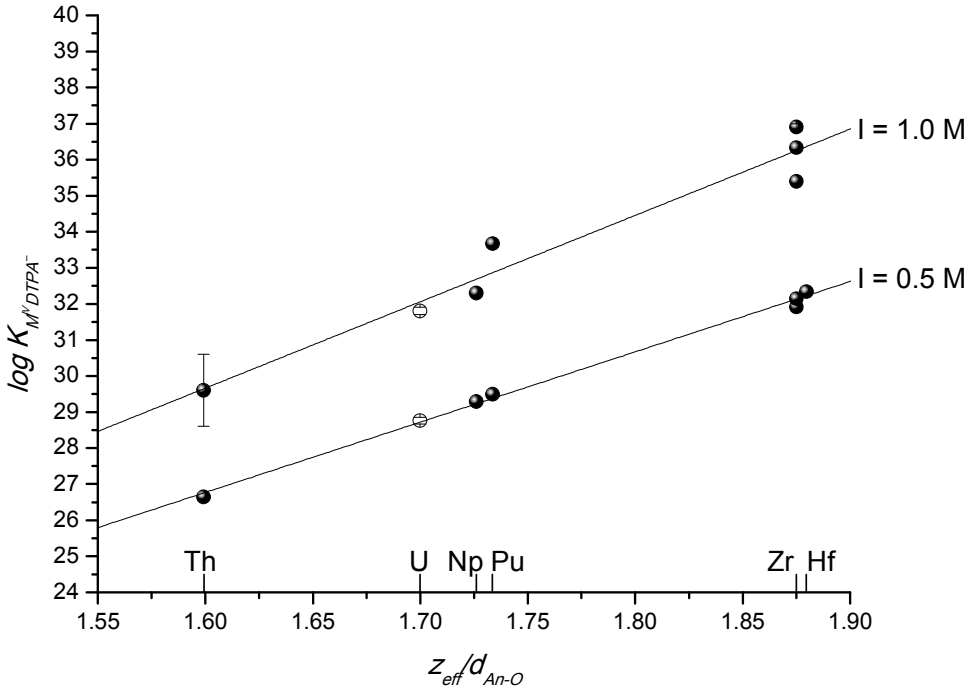

Figure 7: Variation of some $M^{IV}DTPA^-$ stability constants at I = 0.5 M [2-5] or recalculated at I = 0.5 M [42-45] and at I = 1 M [6, 9, 17, 41, 42] as function of the effective charge z_{eff} and the distance oxygen-ligand–metal $d_{An\text{-}O}$. The open point relative to the complex $U^{IV}DTPA^-$ lead to a calculated distance U-O equals to 2.28 ± 0.03 Å (*I* = 0.5 M) and 2.29 ± 0.02 Å (*I* = 1.0 M), respectively.

Table 4: distance Uranium – Oxygen interpolated by 3 calibrated methods and ab initio calculation. The distances $d_{Th\text{-}O}$, $d_{Np\text{-}O}$, and $d_{Pu\text{-}O}$ used for the linear regressions are obtained by *ab initio* molecular dynamics (AIMD).

Method / *linear regression (An=Th, Np, Pu)*	$d_{U\text{-}O}$ (Å)
Thermodynamic / $logK = f(d_{An-O})$	
I = 0.5 M [2, 4, 5]	2.28 ± 0.03
I = 1 M [6]	2.29 ± 0.02
I = 1 M [12]	≈2.30
EXAFS / $d_{An-O} = f(r_{An}^{4+})$*	2.33 ± 0.02
EC-ICPMS / $\Delta\mu = f(d_{An-O})$	
I = 0.05 M	2.32 ± 0.05
I = 0.1 M	2.29 ± 0.02
AIMD / *no calibration*	2.30 ± 0.06

*Coordination Number = 8

Relation electrophoretic mobility – distance ligand-metal. In capillary electrophoresis, the electrophoretic mobility varies with respect on the z/r ratio. The hydrated radius r is of course not equal to the metal-oxygen distance, but it is assumed the contraction of the distance $d_{An\text{-}O}$ induces a proportional volume contraction of the hydrated species. If such assumption is valid, the determination of the distance $d_{An\text{-}O}$ from thermodynamic data and transport ion method (CE) should be the same. It is noted for both methods, a calibration is mandatory to properly interpolate the missing values. The variation of the relative mobility of $An^{IV}DTPA^-$ complexes (reference = $Th^{IV}DTPA^-$)

as a function of $z_{effective}/d_{An\text{-}O}$ is depicted in the Figure 8. The small scattering observed between data is assigned to small changes of the viscosity when pH is adjusted at the desired value. During the experiments, difficulties of detection, i.e. a very small signal compared to that of the other species, were observed for $U^{IV}DTPA^{-}$ probably due to adsorption and/or oxidation process. Only two experiments were useful. The results reported in the Table 4 for CE experiments show an excellent agreement with the other techniques.

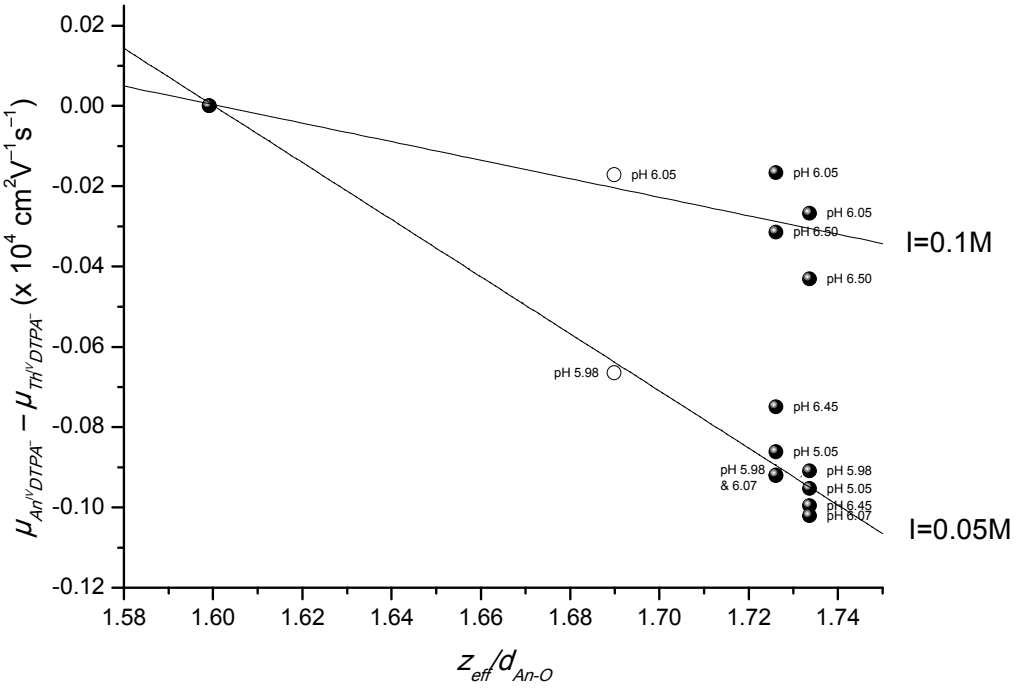

Figure 8: linear trend observed between the relative mobility of $An^{IV}DTPA^{-}$ complexes ($Th^{IV}DTPA^{-}$ = reference) and the ratio $z_{eff}/d_{An\text{-}O}$ for 2 ionic strengths and various pHs. The points relative to the $U^{IV}DTPA^{-}$ species (open circles) are not taken into account for the linear regression.

Predictive capability. The DFT method succeeded in calculating the distances metal–oxygen for thorium, uranium and plutonium and gave values in excellent agreement with the EXAFS experiments. In addition, the evaluation of $d_{U\text{-}O}$ by two other independent methods (thermodynamic and capillary electrophoresis) based on AIMD calibration leads also on an average value in close agreement with the DFT calculation. Based on these successful results, calculation has been extended to transplutonium elements by extrapolation and to protactinium by interpolation. The trend observed in the Figure 7 using data at I = 1.0 M (including U^{IV}) [6], suggests that the stability constants evaluated for Pa^{4+}, Am^{4+}, Bk^{4+} should be: $log\ K_{Pa^{IV}DTPA^{-}}$ = 31.9, $log\ K_{Am^{IV}DTPA^{-}}$ = 34.0, and $log\ K_{Bk^{IV}DTPA^{-}}$ = 33.4. Based on crystallographic data [16] for $Sn^{IV}DTPA^{-}$ complex and the

relation given in Figure 7, the stability constant can also be determined at *I* = 1.0 M: $log\ K_{Sn^{IV}DTPA^{-}}$ = 35.9.

Conclusion

A multi-approach technique combining structural investigations by EXAFS, theoretical calculation by ab initio molecular dynamics, and speciation by hyphenated chromatography-mass spectrometry technique (CE-ICPMS) gave new insight on the stability of the $An^{IV}DTPA^{-}$ chelates. The structure of $An^{IV}DTPA^{-}$ was elucidated for the first time by EXAFS whereas the use of CE-ICPMS in a very uncommon way confirmed the distances obtained by EXAFS. In addition, electronic correlation was taken into account in DFT formalism to properly reproduce the experimental distances. In return, all these techniques have opened the way to a method enabling the evaluation of stability constants. As result, the stability constants of the uncommon chelates $Pa^{IV}DTPA^{-}$, $Am^{IV}DTPA^{-}$, and $Bk^{IV}DTPA^{-}$ have been evaluated.

Acknowledgment

This work was funded under project name DACFAM by the French transverse program “Toxicologie Nucléaire”.

XAS measurements were carried out at ESRF / ROBL, a European synchrotron user facility and at SSRL / 11-2, a national user facility operated by Stanford University on behalf of the U.S. Department of Energy, Office of Basic Energy Sciences. The authors would like to thank for their help Ch. Hennig, A. Rossberg and A. Scheinost on ROBL and S. D. Conradson and J. Rogers on 11-2.

Reference

1. Weaper, B.;F.A. Kappelman: Talspeak: a new method of separating Americium and Curium from the Lanthanides by extraction from an aqueous solution of an aminopolyacetic acid complex with a monoacidic organophosphate or phosphonate, pp. 61. Oak Ridge National Laboratory, Oakridge (1964)
2. Piskunov, E.M.;A.G. Rykov: Investigation of complex formation with diethylenetriaminepentaacetic acid. II. Thorium (IV). Radiokhimiya **14**, 260-265 (1972)
3. Piskunov, E.M.;A.G. Rykov: Investigation of complex formation with diethylenetriaminepentaacetic acid. III. Uranium (IV). Radiokhimiya **14**, 265-268 (1972)
4. Piskunov, E.M.;A.G. Rykov: Investigation of complex formation with diethylenetriaminepentaacetic acid. IV. Neptunium (IV). Radiokhimiya **14**, 330-332 (1972)
5. Piskunov, E.M.;A.G. Rykov: Investigation of complex formation with diethylenetriaminepentaacetic acid. V. Plutonium (IV). Radiokhimiya **14**, 332-333 (1972)
6. Brown, A.;A. Paulenova;A.V. Gelis: Aqueous complexation of thorium(IV), uranium(IV), neptunium(IV), plutonium(III/IV), and cerium(III/IV) with DTPA. Inorg. Chem. **51**, 7741-7748 (2012)
7. Eberle, S.H.;M.T. Paul: Über Aminopolykarbonsäurekomplexe des Np(IV)-Ions. J. Inorg. Nucl. Chem. **33**, 3067-3075 (1971)
8. Bonin, L., *Etude de la spéciation des actinides vis-à-vis de ligands d'intérêt pour la décorporation*, in *Chemistry*. 2008, Université Paris XI: Orsay. p. 135.
9. Bottari, E.;G. Anderegg: Die Untersuchung der 1:1-Komplexe von einigen drei- und vierwertigen Metall-Ionen mit Polyaminocarboxylaten mittels Redoxmessungen. Helv. Chim. Acta **50**, 2349-2356 (1967)
10. Chang, C.T.;M.M. Chang;C.F. Llaw: The behaviors of neptunium in aqueous solutions - III - Stability of DTPA complex. J. Inorg. Nucl. Chem. **35**, 261-264 (1973)
11. Ryabchikov, D.I.;M.P. Volynets: Thorium complexonates. Russ. J. Inorg. Chem. **10**, 334-339 (1965)
12. NIST Standard Reference Database 46, *NIST Critically Selected Stability Constants of Metal Complexes Database*. 2004, U.S. Department of Commerce: Washington, DC.
13. Hseu, T.M.;L. Peng;Z.F. Lin: Spectrophotometric studies of cerium(III) and thorium(IV) chelates of diethylenetriaminepentaacetic acid (DTPA). J. Chinese Chem. Soc. **30**, 159-166 (1983)
14. Grenthe, I.;I. Puigdomenech: Modelling in Aquatic Chemistry. ed, Paris 1997
15. Porai-Koshits, M.A.;L.M. Shkol'nikova;G.G. Sadikov;R.L. Davidovich;V.S. Fundamenskii;V.N. Shchurkina;M.E. Valyaeva: X-ray crystal and molecular structure of guanidinium diethylenetriamine-N,N,N',N'',N''-pentaacetohafnate with nine-coordinated hafnium. Russ. J. Inorg. Chem. **39**, 1724-1733 (1994)
16. Ilyukhin, A.B.;V.S. Sergienko;R.L. Davidovich;V.B. Logvinova: Synthetis and structure of dioxonium diethylenetriaminepentaacetostannate(IV) and diethylenetriaminepentaacetohafnate(IV), H_5O_2[MDTPA] H_2O. Russ. J. Inorg. Chem. **42**, 1341-1345 (1997)
17. Ilyukhin, A.B.;R.L. Davidovich;I.N. Samsonova;L.V. Teplukhina: Eightfold-coordinated diethylenetriaminepentaacetates: crystal structures of K[M(DTPA)] $3H_2O$ (M = Zr or Hf) and NH_4[Sn(Dtpa)] H_2O. Crystallogr. Rep. **45**, 39-43 (2000)
18. Bonin, L.;D. Guillaumont;A. Jeanson;C. Den Auwer;M. Grigoriev;J.C. Berthet;C. Hennig;A. Scheinost;P. Moisy: Thermodynamics and structure of actinide(IV) complexes with nitrilotriacetic acid. Inorg. Chem. **48**, 3943-3953 (2009)
19. Onsager, L.;R.M. Fuoss: Irreversible processes in electrolytes. Diffusion, conductances, and viscous flow in arbitrary mixtures of strong electrolytes. J. Phys. Chem. **36**, 2689-2778 (1932)

20. Jaros, M.;K. Vcelakova;I. Zuskova;B. Gas: Optimization of background electrolytes for capillary electrophoresis: II. Computer simulation and comparison with experiments. Electrophoresis **23**, 2667-2677 (2002)
21. Nightingale, E.R., Jr.: Viscosity of aqueous sodium perchlorate solutions. J. Phys. Chem. **63**, 742-743 (1959)
22. Marcus, Y.: Evaluation of the static permittivity of aqueous electrolytes. J. Solution Chem. **42**, 2354-2363 (2013)
23. Topin, S.;J. Aupiais;N. Baglan;T. Vercouter;P. Vitorge;P. Moisy: Trace metal speciation by capillary electrophoresis hyphenated to inductively coupled plasma mass spectrometry: sulfate and chloride complexes of Np(V) and Pu(V). Anal. Chem. **81**, 5354-5363 (2009)
24. Ravel, B.;M. Newville: ATHENA, ARTEMIS, HEPHAESTUS: data analysis for X-ray absorption spectroscopy using IFEFFIT. J. Synchrotron Rad. **12**, 537-541 (2005)
25. Rehr, J.J.;J.J. Kas;F.D. Vila;M.P. Prange;K. Jorissen: Parameter-free calculations of X-ray spectra with FEFF9. Phys. Chem. Chem. Phys. **12**, 5503-5513 (2010)
26. Gonze, X.;J.M. Beuken;R. Caracas;F. Detraux;M. Fuchs;G.M. Rignanese;L. Sindic;M. Verstraete;G. Zerah;F. Jollet;M. Torrent;A. Roy;M. Mikami;P. Ghosez;J.Y. Raty;D.C. Allan: First-principles computation of material properties: the ABINIT software project. Comput. Mater. Sci. **25**, 478-492 (2002)
27. Koma, H.P.;T.T. Rantala;A. Pasquarello: Finite-size supercell correction schemes for charged defect calculations. Phys. Rev. B **86**, 045112 (2012)
28. Holzwarth, N.A.W.;A.R. Tackett;G.E. Matthews: A Projector Augmented Wave (PAW) code for electronic structure calculations, Part I: atompaw for generating atom-centered functions. Comput. Phys. Commun. **135**, 329-347 (2001)
29. Perdew, J.P.;K. Burke;M. Ernzerhof: Generalized Gradient Approximation Made Simple. Phys. Rev. Lett. **77**, 3865-3868 (1996)
30. Jomard, G.;B. Amadon;F. Bottin;M. Torrent: Structural, thermodynamic, and electronic properties of plutonium oxides from first principles. Phys. Rev. B **78**, 075125 (2008)
31. Gareil, P.: L'électrophorèse de zone et la chromatographie électrocinétique capillaires I. - Principes et notions fondamentales. Analusis **18**, 221-241 (1990)
32. Carey, G.H.;A.E. Martell: Formation, hydrolysis, and olation of uranium(IV) chelates. J. Am. Chem. Soc. **90**, 32-38 (1968)
33. Bogucki, R.F.;A.E. Martell: Hydrolysis and olation of Th(IV) chelates of polyaminocarboxylic acids. J. Am. Chem. Soc. **80**, 4170-4174 (1958)
34. Anderegg, G.;F. Arnaud-Neu;R. Delgado;J. Felcman;K. Popov: Critical evaluation of stability constants of metal complexes of complexones for biomedical and environmental applications. Pure & Appl. Chem. **77**, 1145-1495 (2005)
35. Leguay, S.;T. Vercouter;S. Topin;J. Aupiais;D. Guillaumont;M. Miguirditchian;P. Moisy;C. Le Naour: New Insights into Formation of Trivalent Actinides Complexes with DTPA. Inorg. Chem. **51**, 12638-12649 (2012)
36. Mendes, M.;S. Leguay;C. Le Naour;S. Hamadi;J. Roques;P. Moisy;D. Guillaumont;S. Topin;J. Aupiais;C. Den Auwer;C. Hennig: Thermodynamic Study of the Complexation of Protactinium(V) with Diethylenetriaminepentaacetic Acid. Inorg. Chem. **52**, 7497-7507 (2013)
37. Bénazeth, S.;J. Purans;M.C. Chalbot;M.K. Nguyen-Van-Duong;L. Nicolas;F. Keller;A. Gaudemer: Temperature and pH Dependence XAFS Study of $Gd(DOTA)^-$ and $Gd(DTPA)^{2-}$ Complexes: Solid State and Solution Structures. Inorg. Chem. **37**, 3667-3674 (1998)
38. Robert, G.;A. Pasturel;B. Siberchicot: Structural stability of $Pu_{(1-x)}M_x$ (M=Al, Ga, and In) compounds. Phys. Rev. B **68**, 075109 (2003)
39. Bouchet, J.;B. Siberchicot;F. Jollet;A. Pasturel: Equilibrium properties of $^{\delta}$-Pu: LDA+U calculations (LDA = local density approximation). J. Phys. Condens. Matter **12**, 1723-1733 (2000)

40. Fried, A.R.;A.E. Martell: Structure and conformation of thorium(IV) complexes of diethylenetriaminepentaacetic acid in aqueous solution. J. Am. Chem. Soc. **93**, 4695-4700 (1971)
41. Ermakov, A.N.;I.N. Marov;G.A. Evtikova: Complex formation for zirconium and hafnium with diethylenetriaminepentaacetic acid. Zhur. Neorg. Khim. **9**, 502-505 (1964)
42. Ermakov, A.N.;I.N. Marov;G.A. Evtikova: Zirconium and hafnium complexonates. Zhur. Neorg. Khim. **11**, 1155-1160 (1966)
43. Tikhonova, L.I.: Zirconium complex formation with some polyaminopolyacetic acids. Zhur. Neorg. Khim. **12**, 939-943 (1967)
44. Lapitskii, A.V.;L.N. Pankratova: Reaction of zirconium with some complexons. Vestn. Mosk. Univ. Ser. II Khim. **21**, 61-66 (1966)
45. Pankratova, L.N.;L.G. Vlasov;A.V. Lapitskii: Complex formation of zirconium with DTPA and CHTA. Zhur. Neorg. Khim. **9**, 1363-1368 (1964)
46. Hummel, W.;G. Anderegg;L. Rao;I. Puigdomenech;O. Tochiyama: Chemical Thermodynamics of Compounds and Complexes of U, Np, Pu, Am, Tc, Se, Ni and Zr with Selected Organic Ligands. ed, Amsterdam 2005
47. Bretti, C.;C. De Stefano;C. Foti;S. Sammartano: Acid-base properties, solubility, activity coefficients and Na^+ ion pair formation of complexons in $NaCl_{(aq)}$ at different ionic strengths. J. Sol. Chem. **42**, 1452-1471 (2013)
48. David, F.;V. Vokhmin: Thermodynamic properties of some tri- and tetravalent actinide aquo ions. New J. Chem. **27**, 1627-1632 (2003)
49. Shannon, R.D.: Revised effective ionic radii and systematic studies of interatomic distances in halides and chalcogenides. Acta Cryst. A **32**, 751-767 (1976)

Ab initio molecular dynamic

$$An^{4+} + DTPA^{5-} \rightleftharpoons AnDTPA^{-}$$

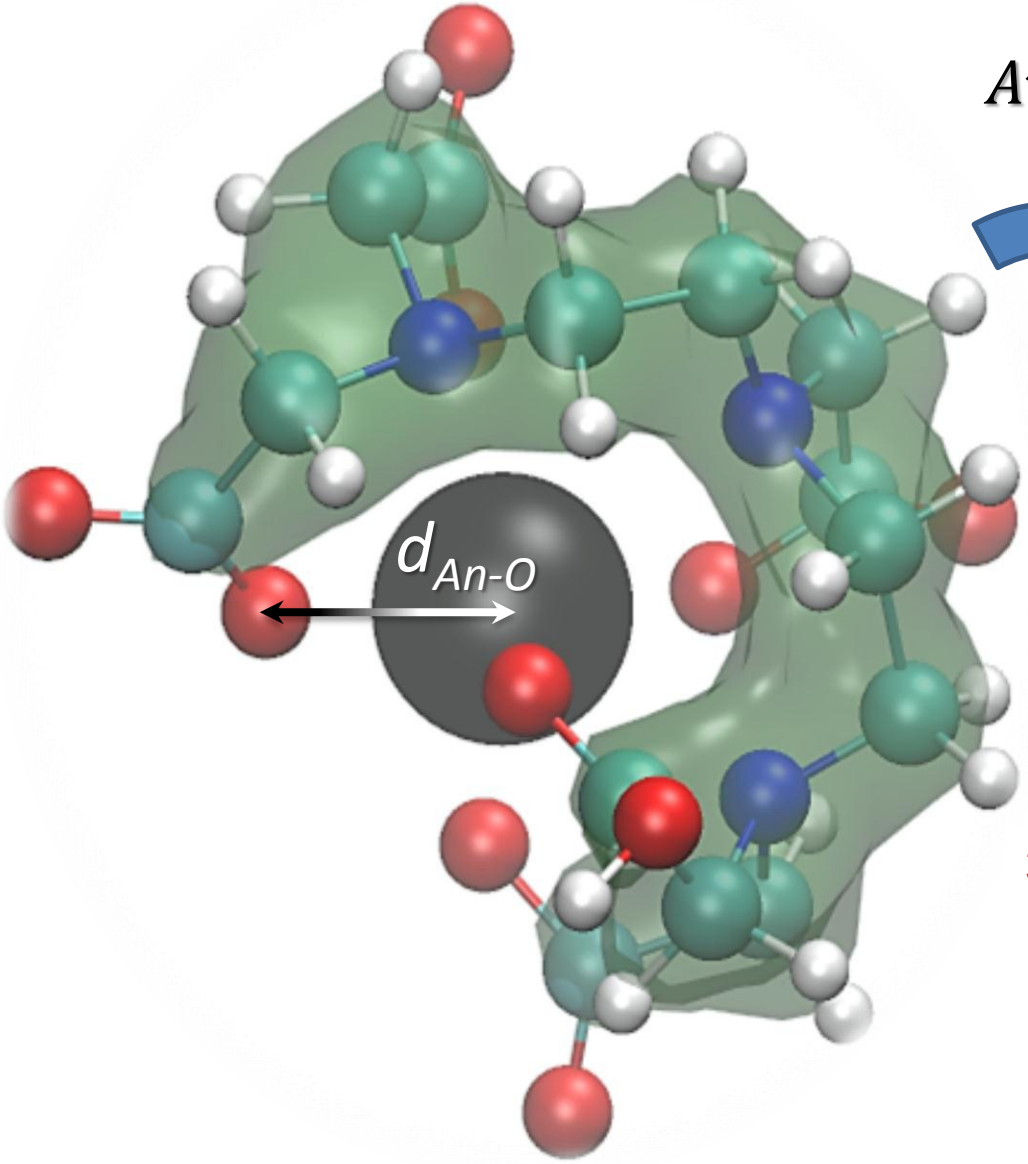

Prediction